ARTICLES
https://doi.org/10.1038/s41561-018-0227-0

nature geoscience

Corrected: Author Correction

Path-dependent reductions in CO_2 emission budgets caused by permafrost carbon release

T. Gasser[1*], M. Kechiar[1,2], P. Ciais[3], E. J. Burke[4], T. Kleinen[5], D. Zhu[3], Y. Huang[3], A. Ekici[6,7] and M. Obersteiner[1]

Emission budgets are defined as the cumulative amount of anthropogenic CO_2 emission compatible with a global temperature-change target. The simplicity of the concept has made it attractive to policy-makers, yet it relies on a linear approximation of the global carbon–climate system's response to anthropogenic CO_2 emissions. Here we investigate how emission budgets are impacted by the inclusion of CO_2 and CH_4 emissions caused by permafrost thaw, a non-linear and tipping process of the Earth system. We use the compact Earth system model OSCAR v2.2.1, in which parameterizations of permafrost thaw, soil organic matter decomposition and CO_2 and CH_4 emission were introduced based on four complex land surface models that specifically represent high-latitude processes. We found that permafrost carbon release makes emission budgets path dependent (that is, budgets also depend on the pathway followed to reach the target). The median remaining budget for the 2 °C target reduces by 8% (1–25%) if the target is avoided and net negative emissions prove feasible, by 13% (2–34%) if they do not prove feasible, by 16% (3–44%) if the target is overshot by 0.5 °C and by 25% (5–63%) if it is overshot by 1 °C. (Uncertainties are the minimum-to-maximum range across the permafrost models and scenarios.) For the 1.5 °C target, reductions in the median remaining budget range from ~10% to more than 100%. We conclude that the world is closer to exceeding the budget for the long-term target of the Paris Climate Agreement than previously thought.

Sometimes called 'carbon budgets', cumulative anthropogenic CO_2 emission budgets compatible with a given global mean warming target have been evaluated in many ways[1–10]. Yet, only a handful of the studies[11–13] made (incomplete) preliminary attempts to account for permafrost thaw. The additional emission of CO_2 and CH_4 caused by this natural process triggered by warming in the high latitudes[13,14] will diminish the budget of CO_2 humankind can emit to keep below a certain level of global warming. Permafrost carbon release is also an irreversible process over the course of a few centuries[13,14], and may thus be considered a 'tipping' element of the Earth's carbon–climate system[15], which puts the linear approximation of the emission budget framework[1,4,5,16,17] to the test.

To quantify the impact of permafrost carbon release on emission budgets, we use an Earth system model of reduced complexity whose processes are parameterized to faithfully emulate more complex models. OSCAR v2.2.1 (a minor update of v2.2 (ref. [18])) was run in its default configuration, which is comparable to the median of its probabilistic set-up. Therefore, all our results are for about a 50% chance of meeting the temperature targets. OSCAR is extended here with a new permafrost carbon module that emulates four state-of-the-art land surface models: JSBACH (Methods), ORCHIDEE-MICT (ref. [19]), and two versions of JULES (refs [20,21]). These complex models were developed specifically to represent high-latitude processes, in particular soil thermic and biogeochemistry mechanisms that control carbon sequestration and emission. In this new emulator, the permafrost carbon in two high-latitude regions is represented as an initially frozen pool that thaws as global temperature increases. Thawed carbon is not immediately emitted: it is split between several pools, each with its specific timescale of emission. We assume that 2.3% of the emission occurs as methane[14] (Methods discusses the uncertainty of this value), and this emitted CH_4 is fully coupled to the dynamical atmospheric chemistry of OSCAR. More details on the protocol, the emulator and the models are provided in Methods.

We do not assume a priori that reductions in emission budgets can simply be calculated as the cumulative permafrost carbon release in a given scenario. Quite the opposite, we apply three specifically designed approaches to estimate emission budgets. The first one is the 'exceedance' approach, in which the budget is a threshold in terms of cumulative anthropogenic CO_2 emissions above which the temperature target is exceeded (with a given probability). The second one is the 'avoidance' approach, in which the budget is another—typically lower—cumulative emissions threshold below which the target is avoided (also with a given probability). These two approaches were used in the fifth International Panel on Climate Change (IPCC) assessment report[6,22]. However, neither of these considers the possibility of overshooting the target first, and then returning below it afterwards. To investigate such a case, we adapted the approach of MacDougall et al.[12] to create 'overshoot' budgets.

Reductions in exceedance and avoidance budgets. With the exceedance approach, budgets are calculated in any given scenario as the maximum cumulative CO_2 emissions before the point in time when global temperature reaches the target level for the first time. This is illustrated in Fig. 1 (Methods and example given in Supplementary Fig. 1). Here our exceedance budgets are based on the four extended representative concentration pathways (RCP) emission scenarios[23] and two idealized scenarios (Methods and Supplementary Fig. 2).

When permafrost carbon is ignored, we estimated total exceedance budgets of 2,350 (2,290–2,480) Gt CO_2 for the 1.5 °C target and

[1]International Institute for Applied Systems Analysis (IIASA), Laxenburg, Austria. [2]École Polytechnique, Palaiseau, France. [3]Laboratoire des Sciences du Climat et de l'Environnement, LSCE/IPSL, Université Paris-Saclay, CEA – CNRS – UVSQ, Gif-sur-Yvette, France. [4]Met Office Hadley Centre, Exeter, UK. [5]Max Planck Institut für Meteorologie, Hamburg, Germany. [6]Climate and Environmental Physics, Physics Institute, University of Bern, Bern, Switzerland. [7]Oeschger Centre for Climate Change Research, University of Bern, Bern, Switzerland. *e-mail: gasser@iiasa.ac.at

3,260 (3,110–3,550) Gt CO_2 for 2 °C, with 1870 as the preindustrial reference year (Supplementary Table 1, which also contains budgets for 2.5 °C and 3 °C). (Uncertainties are the minimum-to-maximum range across the permafrost models and scenarios.) Our results are ~3% different from the IPCC estimates based on complex models[6]. This confirms that OSCAR's default configuration gives results consistent with the Earth system models used in previous climate change assessments.

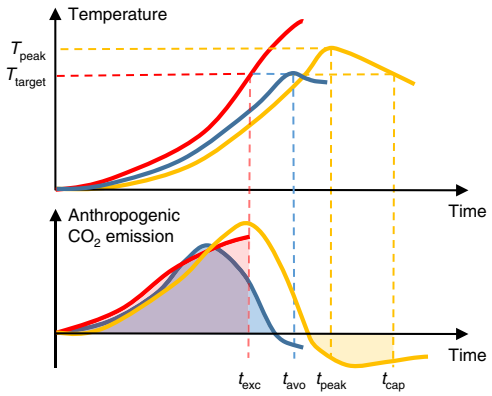

Fig. 1 | Illustration of the three budget-calculation approaches used in this study. Exceedance budgets (red) are the amount of CO_2 that can be emitted before exceeding a given temperature target. Avoidance budgets (blue) are the amount of CO_2 that can be emitted while staying below the target. Capture budgets (yellow) are the amount of CO_2 that needs be captured when the target temperature is overshot by a given level. Capture budgets are combined with avoidance budgets to give the net overshoot budgets. Methods and Supplementary Fig. 1 give technical details on how these budgets are calculated. t_{exc} is the time at which the target is exceeded (for exceedance budgets), t_{avo} is when temperature peaks at the targeted level (for avoidance budgets), t_{peak} is when temperature peaks at a given overshooting level above the targeted level (for overshoot budgets) and t_{cap} is when temperature returns below the targeted level (for capture budgets and hence also overshoot budgets).

When permafrost carbon processes are included, exceedance budgets are reduced by 30 (10–120) Gt CO_2 for 1.5 °C and 60 (10–200) Gt CO_2 for 2 °C (Fig. 2a and Supplementary Table 1). This is only a few percentage points of the total budgets, but it corresponds to a more substantial reduction in the remaining budgets (Fig. 2b). It is also smaller in magnitude than previously estimated with a model of intermediate complexity[12], which can be explained by the oversensitivity of the permafrost carbon model used in that study (Table 1). An important (known) caveat of the exceedance approach is that it ignores the system's dynamics after the point in time at which the temperature target is reached[22]. This is especially important for permafrost carbon, as a significant part of the thawed carbon keeps being emitted long after the target is first reached (Supplementary Fig. 3), which implies the temperature target will actually be surpassed if budgets are based on this approach.

With the avoidance approach, budgets are calculated using a large ensemble of peak-and-decline emission scenarios whose values of peak temperature and maximum cumulative CO_2 emissions are used for interpolation (Fig. 1, Methods and Supplementary Fig. 1). This approach accounts for the complete system's dynamic by ensuring that the temperature target is never exceeded. Its drawback, however, is its intense computing requirement that makes it extremely costly to follow by complex models. Here we create and use an ensemble of 3,120 scenarios, by combining 520 fossil fuel CO_2 emission scenarios of our own making (Supplementary Fig. 4) to the land-use and non-CO_2 climate forcers from the six scenarios previously used for exceedance budgets (Methods).

Permafrost carbon reduces avoidance budgets by 60 (10–180) Gt CO_2 for 1.5 °C and 100 (20–270) Gt CO_2 for 2 °C (Fig. 2a). This reduction in avoidance budgets is systematically larger than for exceedance budgets: by 20% to 140% across all the emulated permafrost carbon models (Fig. 3). This confirms that the exceedance approach only partially captures the impact of permafrost carbon release on emission budgets. We conjecture that other slow and strongly non-linear processes, such as forest dieback[15,24,25], are also incompletely accounted for with exceedance budgets. As the exceedance approach was the only one used by complex models in the fifth IPCC assessment report[6,22], we conclude that future updates

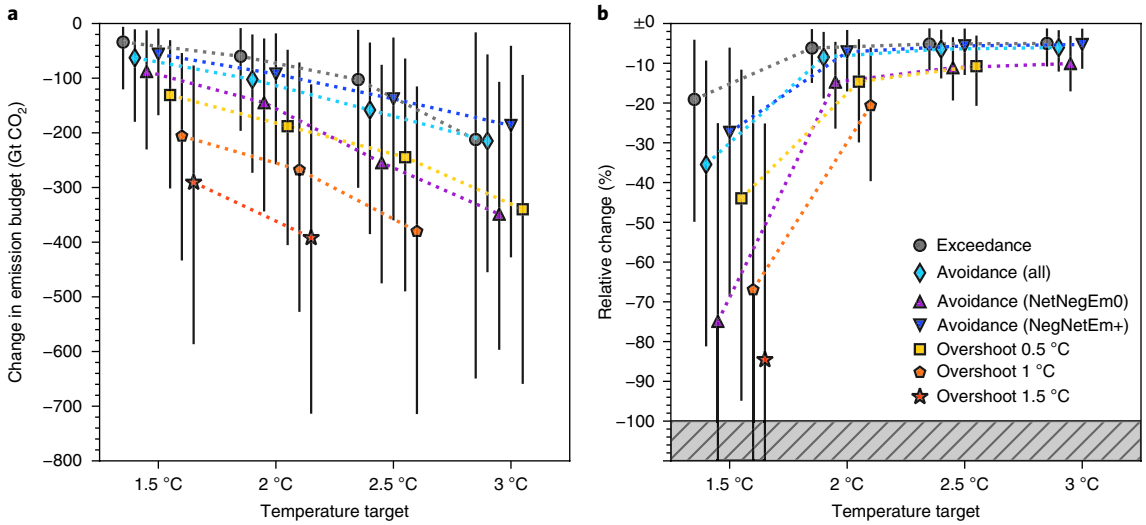

Fig. 2 | Change in emission budgets caused by permafrost carbon release. The different budget-calculation approaches include different levels of overshoot and the avoidance budgets based on two subgroups of scenarios: NetNegEm0 and NetNegEm+. The uncertainty bars show the full range and the symbols show the average, across all permafrost models and scenarios. **a**, Absolute reductions in emission budgets. **b**, Relative reductions in the remaining budgets, calculated by assuming 2,240 Gt CO_2 (ref. [44]) was emitted between 1870 (the preindustrial reference year) and 2017 (Methods). To better isolate the effect of permafrost carbon in **b**, we present values under a constant present-day non-CO_2 radiative forcing (other non-CO_2 backgrounds are available in Supplementary Table 1). The grey hashed area represents a permafrost-induced reduction of 100% or more, which would imply that the budget was already exceeded in 2017.

Table 1 | Comparison of cumulative permafrost carbon release estimated in 2100, 2200 and 2300 (Pg C (1 Pg C = $\frac{44}{12}$ Gt CO_2))

Reference	2100	2200	2300	Notes
High-emission scenarios: RCP8.5 or SRES A2				
This study	59 (11–143)	150 (34–297)	212 (55–376)	–
Koven et al.[30]	57 (28–113)	–	–	Data-constrained modelling
MacDougall et al.[12]	226	611	–	CO_2-only simulations
Schuur et al.[14]	37–174	–	Approx. 100–400	Review that compiled several studies
Schaefer et al.[13]	37–347	–	–	Review that compiled several studies
Medium–high stabilization scenarios: RCP6.0 or SRES A1B				
This study	42 (8–102)	99 (23–203)	145 (39–265)	–
MacDougall et al.[12]	166	–	–	CO_2-only simulations
Schaefer et al.[11]	–	190 ± 24	–	Uncertainty is 1σ
Medium–low stabilization scenario: RCP4.5				
This study	35 (7–83)	64 (16–130)	89 (26–163)	–
Koven et al.[30]	21 (12–33)	–	–	Data-constrained modelling
MacDougall et al.[12]	156	–	–	CO_2-only simulations
Schaefer et al.[13]	27–100	–	–	Review that compiled several studies
Low-emission scenario: RCP2.6				
This study	27 (6–62)	39 (11–82)	47 (15–93)	–
MacDougall et al.[12]	103	153	169	CO_2-only simulations

Uncertainties show the full range of simulations or studies, unless noted otherwise. A more comprehensive comparison that includes other data[26,48,49] is provided in Supplementary Table 3.

of the emission budgets based on such models will remain biased without a change in experimental protocol.

Path dependency and overshooting pathways. Our ensemble of 3,120 scenarios for the avoidance budgets covers a large enough spectrum of possible futures that it can be split into two groups (Methods and Supplementary Fig. 4). In the subgroup of scenarios that have no net negative emissions (NetNegEm0), the permafrost-induced reduction in avoidance budgets is 90 (10–230) Gt CO_2 for 1.5 °C and 150 (30–340) Gt CO_2 for 2 °C (Fig. 2a). This is systematically more than in the subgroup of scenarios in which the net negative emissions are extensively implemented (NetNegEm+) (Fig. 3). The physical reason for this is that extensive net negative emissions artificially make the temperature peak a few years after they are introduced, whereas when net negative emissions are not available the peak of the temperature is caused by natural processes only, and permafrost carbon emissions can delay it for decades (Supplementary Fig. 5). That the effect of permafrost carbon release depends on the emission pathway is proof that inclusion of such a previously unaccounted for tipping process renders emission budgets path dependent. In other words, the emission budget compatible with a given target depends on both the timing and magnitude of the anthropogenic emissions, and not on their magnitude alone.

To investigate this path dependency further, we looked into overshoot budgets using the same ensemble of scenarios as for those avoidance budgets (Methods). The net overshoot budgets were calculated as the sum of two gross budgets: a 'peak' budget that is exactly the same as an avoidance budget for a given peak temperature above the long-term target, and a 'capture' budget that corresponds to the amount of net negative emission required to return below the long-term temperature target (Fig. 1, Methods and Supplementary Fig. 1). Capture budgets have a mathematical

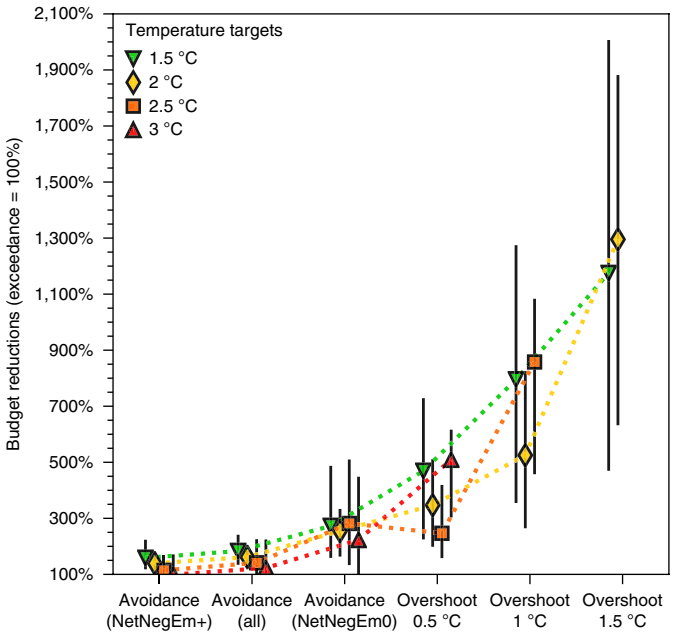

Fig. 3 | Path dependency of the permafrost-induced budget reductions. Reductions in avoidance and overshoot budgets are compared to reductions in exceedance budgets (reference case of 100%). Each type of budget represents a different archetype of pathway, and they are roughly sorted by the increasing intensity of the permafrost effect. The uncertainty bars show the full range of our results. Values >100% mean that the emission budgets are more largely reduced than in the exceedance case. If the permafrost effect was path independent, all the points would be close to 100%.

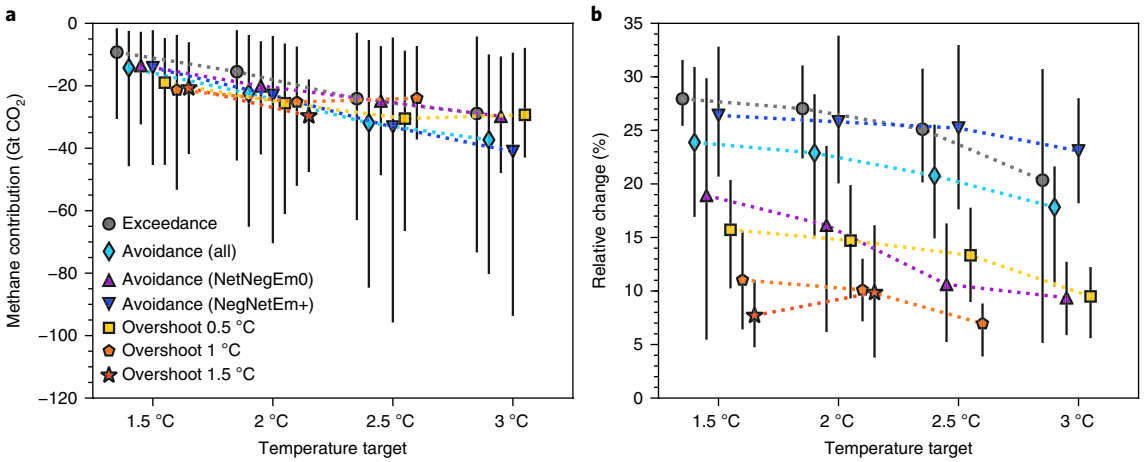

Fig. 4 | Contribution of CH_4 released by permafrost thaw to the budget reductions. a,**b**, Absolute (**a**) and relative (**b**) terms with regard to the values shown in Fig. 2a. Uncertainty bars show the full range and symbols show the average, across all permafrost models and scenarios.

definition analogous to exceedance budgets, and so these budgets have the same caveat of overlooking the system's evolution after the target is met. Longer-term requirements in CO_2 capture to compensate for lasting permafrost emissions[26,27] are therefore ignored in our capture budgets (provided in Supplementary Table 2). Also, only net negative emission requirements can be estimated in this way—gross negative emissions could be much larger if the decrease in fossil fuel consumption was not rapid enough[28].

In the case of an overshoot amplitude of 0.5 °C, emissions from permafrost thaw reduce the net emission budgets by 130 (30–300) Gt CO_2 for the 1.5 °C long-term target (that is for a peak temperature of 2 °C, a case that corresponds to the Paris Climate Agreement), and by 190 (50–400) Gt CO_2 for the 2 °C target (Fig. 2a). For an overshoot amplitude of 1 °C, permafrost-induced reductions reach 210 (50–430) Gt CO_2 for the 1.5 °C target, and 270 (70–530) Gt CO_2 for 2 °C target. (Budgets for other targets and other levels of overshoot are provided in Fig. 2 and Supplementary Table 1.) The permafrost-induced reduction is systematically more pronounced in these cases than in non-overshooting scenarios (Fig. 3) because of the additional capture required to counteract the extra emission from the thawed permafrost that occurs during the overshoot period. It is already known that the rest of the carbon–climate system (that is, excluding permafrost) exhibits a path-dependent behaviour under overshooting scenarios[29] (Supplementary Fig. 6), but our results show that permafrost carbon release strongly reinforces this rupture of the linear approximation of the emission budget framework.

Discussion and policy implications. A permafrost-induced path dependency of emission budgets was implied by MacDougall et al.[12], although their quantification of the effect was biased by the high sensitivity of their model's permafrost carbon release in response to high-latitude warming (Table 1; note that an update of their model showed a lower bias[26]). Their study also focused on exceedance budgets and a handful of overshooting scenarios that did not correspond to political commitments. The Paris Climate Agreement aims to avoid 2 °C, which implies avoidance budgets are needed. It also recognizes an overshooting trajectory by setting the long-term target to 1.5 °C, which means overshoot budgets are also needed.

A few earlier attempts to quantify the permafrost-induced reduction in emission budgets were also made[11,13], albeit without applying any of the budget-calculation approaches we use. They simply subtracted cumulative emissions caused by permafrost thaw from cumulative anthropogenic emissions at an arbitrary point in time. Such an approach is not suitable to estimate budget reductions accurately (Supplementary Fig. 7) because it overlooks the dynamical response of the coupled system. It was not retained in the fifth IPCC assessment report[6]. Additionally, these earlier studies did not find path dependency, either because only one scenario was investigated[11] or because path independency was assumed[13].

The OSCAR v2.2.1 model, with its new permafrost carbon emulator, estimates future carbon release from thawing permafrost within the range of existing studies (Table 1). A cumulative 60 (11–144) Pg C is projected to be released by 2100 under RCP8.5, slightly lower than the 37–174 Pg C reviewed by Schuur et al.[14], and close to the 28–113 Pg C obtained with a data-constrained model by Koven et al.[30]. Uncertainties in permafrost-related processes and their response to climate change remain very high, however, and there are elements that suggest our results are conservative. Deep (for example, Yedoma) and seabed permafrost thaw is not modelled. Should these carbon stocks be mobilized, budgets would be further reduced. Changes in the nitrogen cycling caused by permafrost thaw are also ignored. These could lead to the emission of N_2O (ref. [31]), but also to changes in the ecosystems' net carbon balance[32].

We also assume a constant fraction of permafrost carbon is emitted as CH_4, but the value and future evolution of this fraction are uncertain[14,33,34]. With this constant value, we simulate an emission of 3.7 (0.7–10.5) Tg CH_4 per year over the 1980–2012 period, in line with a recent review[35]. This methane contributes a non-negligible fraction of the reduction in emission budgets (Fig. 4). This contribution is also path dependent, contrary to that obtained in previous studies[13,33] by using a fixed global warming potential. It is, however, a well-known caveat of global warming potentials (or any other emission metric) that they are linear and constant, whereas the actual Earth system behaves in a complex, dynamical and non-linear fashion[36–39], and so they cannot be naively used in combination with emission budgets[40].

These uncertainty sources mean we assume that no probabilistic distribution of the permafrost-induced effect can yet be drawn from our results, and so we provide its full range. To reduce this uncertainty, it is key to foster observation- and model-based research on the permafrost and other tipping processes of the Earth system so as to know if and when the world will enter an overshooting climatic regime. Meanwhile, permafrost adds to the uncertain context under which climate policy decisions must be taken[41–43]. Careful policy-making might entail taking the pessimistic end of our estimates.

Nevertheless, we showed here that accounting for the tipping elements of the Earth system breaks the apparent linear behaviour of the carbon–climate system, which equates to making emission budgets path dependent. This renders manipulating budgets more delicate

than previously thought, as budget users have to make assumptions regarding the long-term target, but also the shorter-term target (for example, the risk of overshooting) and even the reliance on certain technologies (as we demonstrate for net negative emissions).

Furthermore, we quantified a substantial permafrost-induced reduction in the remaining budgets for low-warming targets. This ranges from ~5% to as much as ~40% for a 2 °C target, and from ~10% to more than 100% for a 1.5 °C one, under present-day non-CO_2 forcing and for an about 50% chance of meeting the temperature targets. Whether the world has already breached the budget for 1.5 °C remains elusive, however. It depends on many factors which include the uncertainty on past anthropogenic emissions[44,45], the amount of forcing by non-CO_2 species that will be mitigated in the near future[12,46,47] and a possible bias in the model's simulated present-day global temperature[7–10] (not accounted for in this study). Irrespective of these uncertainties, it appears that the attainability of the Paris Climate Agreement is more compromised than suggested by the existing literature that largely ignores tipping or irreversible feedbacks of the Earth system.

Online content

Any methods, additional references, Nature Research reporting summaries, source data, statements of data availability and associated accession codes are available at https://doi.org/10.1038/s41561-018-0227-0.

Received: 8 June 2018; Accepted: 14 August 2018;
Published online: 17 September 2018

References

1. Matthews, H. D., Gillett, N. P., Stott, P. A. & Zickfeld, K. The proportionality of global warming to cumulative carbon emissions. *Nature* **459**, 829–832 (2009).
2. Zickfeld, K., Eby, M., Matthews, H. D. & Weaver, A. J. Setting cumulative emissions targets to reduce the risk of dangerous climate change. *Proc. Natl Acad. Sci. USA* **106**, 16129–16134 (2009).
3. Steinacher, M., Joos, F. & Stocker, T. F. Allowable carbon emissions lowered by multiple climate targets. *Nature* **499**, 197–201 (2013).
4. Allen, M. R. & Stocker, T. F. Impact of delay in reducing carbon dioxide emissions. *Nat. Clim. Change* **4**, 23–26 (2014).
5. Friedlingstein, P. et al. Persistent growth of CO_2 emissions and implications for reaching climate targets. *Nat. Geosci.* **7**, 709–715 (2014).
6. IPCC *Climate Change 2014: Synthesis Report* (eds Core Writing Team, Pachauri, R. K. & Meyer L. A.) (IPCC, 2015).
7. Millar, R. J. et al. Emission budgets and pathways consistent with limiting warming to 1.5 °C. *Nat. Geosci.* **10**, 741–747 (2017).
8. Schurer, A. P. et al. Interpretations of the Paris climate target. *Nat. Geosci.* **11**, 220–221 (2018).
9. Tokarska, K. B. & Gillett, N. P. Cumulative carbon emissions budgets consistent with 1.5 °C global warming. *Nat. Clim. Change* **8**, 296–299 (2018).
10. Goodwin, P. et al. Pathways to 1.5 °C and 2 °C warming based on observational and geological constraints. *Nat. Geosci.* **11**, 102–107 (2018).
11. Schaefer, K., Zhang, T., Bruhwiler, L. & Barrett, A. P. Amount and timing of permafrost carbon release in response to climate warming. *Tellus B* **63**, 165–180 (2011).
12. MacDougall, A. H., Zickfeld, K., Knutti, R. & Matthews, H. D. Sensitivity of carbon budgets to permafrost carbon feedbacks and non-CO_2 forcings. *Environ. Res. Lett.* **10**, 125003 (2015).
13. Schaefer, K., Lantuit, H., Romanovsky, V. E., Schuur, E. A. G. & Witt, R. The impact of the permafrost carbon feedback on global climate. *Environ. Res. Lett.* **9**, 085003 (2014).
14. Schuur, E. A. G. et al. Climate change and the permafrost carbon feedback. *Nature* **520**, 171–179 (2015).
15. Lenton, T. M. et al. Tipping elements in the Earth's climate system. *Proc. Natl Acad. Sci. USA* **105**, 1786–1793 (2008).
16. Allen, M. R. et al. Warming caused by cumulative carbon emissions towards the trillionth tonne. *Nature* **458**, 1163–1166 (2009).
17. Zickfeld, K., Arora, V. K. & Gillet, N. P. Is the climate response to CO_2 emissions path dependent?. *Geophys. Res. Lett.* **39**, L05703 (2012).
18. Gasser, T. et al. The compact Earth system model OSCARv2.2: description and first results. *Geosci. Model Dev.* **10**, 271–319 (2017).
19. Guimberteau, M. et al. ORCHIDEE-MICT (v8.4.1), a land surface model for the high latitudes: model description and validation. *Geosci. Model Dev.* **11**, 121–163 (2018).
20. Burke, E. J., Chadburn, S. E., & Ekici, A. A vertical representation of soil carbon in the JULES land surface scheme (vn4.3_permafrost) with a focus on permafrost regions. *Geosci. Model Dev.* **10**, 959–975 (2017).
21. Burke, E. J. et al. Quantifying uncertainties of permafrost carbon–climate feedbacks. *Biogeosciences* **14**, 3051–3066 (2017).
22. Rogelj, J. et al. Differences between carbon budget estimates unravelled. *Nat. Clim. Change* **6**, 245–252 (2016).
23. Meinshausen, M. et al. The RCP greenhouse gas concentrations and their extensions from 1765 to 2300. *Clim. Change* **109**, 213–241 (2011).
24. Cramer, W. et al. Global response of terrestrial ecosystem structure and function to CO_2 and climate change: results from six dynamic global vegetation models. *Global Change Biol.* **7**, 357–373 (2001).
25. Huntingford, C. et al. Simulated resilience of tropical rainforests to CO_2-induced climate change. *Nat. Geosci.* **6**, 268–273 (2013).
26. MacDougall, A. H., & Knutti, R. Projecting the release of carbon from permafrost soils using a perturbed parameter ensemble modelling approach. *Biogeosciences* **13**, 2123–2136 (2016).
27. Burke, E. J., Chadburn, S. E., Huntingford, C. & Jones, C. D. CO_2 loss by permafrost thawing implies additional emissions reductions to limit warming to 1.5 or 2 °C. *Environ. Res. Lett.* **13**, 024024 (2018).
28. Gasser, T., Guivarch, C., Tachiiri, K., Jones, C. D. & Ciais, P. Negative emissions physically needed to keep global warming below 2 °C. *Nat. Commun.* **6**, 7958 (2015).
29. Zickfeld, K., MacDougall, A. H. & Matthews, H. D. On the proportionality between global temperature change and cumulative CO_2 emissions during periods of net negative CO_2 emissions. *Environ. Res. Lett.* **11**, 055006 (2016).
30. Koven, C. D. et al. A simplified, data-constrained approach to estimate the permafrost carbon–climate feedback. *Phil. Trans. R. Soc. A* **373**, 20140423 (2015).
31. Voigt, C. et al. Increased nitrous oxide emissions from Arctic peatlands after permafrost thaw. *Proc. Natl Acad. Sci. USA* **114**, 6238–6243 (2017).
32. Mack, M. C., Schuur, E. A. G., Bret-Harte, M. S., Shaver, G. R. & Chapin, F. S. Ecosystem carbon storage in arctic tundra reduced by long-term nutrient fertilization. *Nature* **431**, 440–443 (2004).
33. Schuur, E. A. G. et al. Expert assessment of vulnerability of permafrost carbon to climate change. *Clim. Change* **119**, 359–374 (2013).
34. Schädel, C. et al. Potential carbon emissions dominated by carbon dioxide from thawed permafrost soils. *Nat. Clim. Change* **6**, 950–953 (2016).
35. Nzotungicimpaye, C.-M. & Zickfeld, K. The contribution from methane to the permafrost carbon feedback. *Curr. Clim. Change Rep.* **3**, 58–68 (2017).
36. Myhre, G. et al. in *Climate Change 2013: The Physical Science Basis* (eds Stocker, T. F. et al.) Ch. 8, 659–740 (IPCC, Cambridge Univ. Press, Cambridge, 2013).
37. Pierrehumbert, R. T. Short-lived climate pollution. *Annu. Rev. Earth. Planet. Sci.* **42**, 341–379 (2014).
38. Shine, K. P., Allan, R. P., Collins, W. J., & Fuglestvedt, J. S. Metrics for linking emissions of gases and aerosols to global precipitation changes. *Earth Syst. Dynam* **6**, 525–540 (2015).
39. Gasser, T. et al. Accounting for the climate–carbon feedback in emission metrics. *Earth Syst. Dynam* **8**, 235–253 (2017).
40. Allen, M. R. et al. New use of global warming potentials to compare cumulative and short-lived climate pollutants. *Nat. Clim. Change* **6**, 773–776 (2016).
41. Kunreuther, H. et al. Risk management and climate change. *Nat. Clim. Change* **3**, 447–450 (2013).
42. Hall, J. W. et al. Robust climate policies under uncertainty: a comparison of robust decision making and info-gap methods. *Risk Anal.* **32**, 1657–1672 (2012).
43. Hallegatte, S. Strategies to adapt to an uncertain climate change. *Global Environ. Change* **19**, 240–247 (2009).
44. Le Quéré, C. et al. Global carbon budget 2017. *Earth Syst. Sci. Data* **10**, 405–448 (2018).
45. Quilcaille, Y. et al. Uncertainty in projected climate change arising from uncertain fossil-fuel emission factors. *Environ. Res. Lett.* **13**, 044017 (2018).
46. Rogelj, J. et al. Disentangling the effects of CO_2 and short-lived climate forcer mitigation. *Proc. Natl Acad. Sci. USA* **111**, 16325–16330 (2014).
47. Shindell, D. et al. Simultaneously mitigating near-term climate change and improving human health and food security. *Science* **335**, 183–189 (2012).
48. Schneider von Deimling, T. et al. Estimating the near-surface permafrost-carbon feedback on global warming. *Biogeosciences* **9**, 649–665 (2012).
49. Schneider von Deimling, T. et al. Observation-based modelling of permafrost carbon fluxes with accounting for deep carbon deposits and thermokarst activity. *Biogeosciences* **12**, 3469–3488 (2015).

Acknowledgements

We thank A. H. MacDougall for sharing data and O. Boucher for data used in Supplementary Fig. 6. This work is part of the European Research Council Synergy project 'Imbalance-P' (grant no. ERC-2013-SyG-610028). Simulations with OSCAR were carried out on the IPSL Prodiguer-Ciclad facility, which is supported by CNRS, UPMC

and Labex L-IPSL, and funded by the ANR (grant no. ANR-10-LABX-0018) and the European FP7 IS-ENES2 project (grant no. 312979). E.J.B. was supported by PAGE21 (EU project no. GA282700), CRESCENDO (EU project no. 641816) and the Joint UK DECC/Defra Met Office Hadley Centre Climate Programme (GA01101). A.E. was also supported by PAGE21.

Author contributions

T.G. designed the study. T.G. developed the permafrost emulator with inputs from P.C. and M.K. T.K. provided JSBACH data. Y.H., D.Z. and P.C. provided ORCHIDEE data. E.J.B. and A.E. provided JULES data. T.G. and M.K. set up the simulations with OSCAR, processed the outputs and created the figures. T.G., M.K., P.C. and M.O. discussed the preliminary results. T.G. wrote the manuscript with contributions from all the authors.

Competing interests

The authors declare no competing interests.

Additional information

Supplementary information is available for this paper at https://doi.org/10.1038/s41561-018-0227-0.

Reprints and permissions information is available at www.nature.com/reprints.

Correspondence and requests for materials should be addressed to T.G.

Publisher's note: Springer Nature remains neutral with regard to jurisdictional claims in published maps and institutional affiliations.

Methods

OSCAR v2.2.1. OSCAR is a compact Earth system model whose modules are calibrated to emulate the behaviour of more complex models[18]. Of particular interest to this study, OSCAR features a module for the terrestrial carbon cycle calibrated on TRENDY and CMIP5 data[50,51], a module for the oceanic carbon cycle adapted from the literature[52] to embed CMIP5 data[51], a climate-response module calibrated on CMIP5 models[53] and an atmospheric chemistry module for the CH_4 tropospheric lifetime[54].

We used OSCAR v2.2.1, which is a minor update of v2.2. The only change between the two versions that affects this study is a minor correction of the carbonate chemistry in the surface ocean. This correction implies a better behaviour of the model for high-warming scenarios. All the equations remain the same as in the description paper[18].

We used the global RCP data[23] to drive the model over the data set's historical period (1765–2005) and following the four extended RCP scenarios (2006–2500). Concentrations of all the greenhouse gases but CO_2 and CH_4 are prescribed to the model. Radiative forcings (RFs) of all the near-term climate forcers (ozone and aerosols) and albedo effects (black carbon on snow and land-cover change) are also prescribed. Therefore, the model was run in an emission-driven fashion only for fossil CO_2 and CH_4 emissions. However, to ensure that we obtained the same atmospheric concentrations of CO_2 and CH_4 as those of the RCPs when permafrost thaw is turned off, we first ran a concentration-driven simulation which we used to back-calculate the anthropogenic emissions of CO_2 and CH_4 that are compatible with these atmospheric concentrations[28,55]. These compatible anthropogenic emissions were then used to drive the model, instead of the original RCP emissions. Land-use and land-cover change data come from the LUH1.1 data set[56] up to 2100. After that year, land-cover change is assumed to be zero, and land uses (wood harvest and shifting cultivation) are assumed to be constant.

We also introduced the CST and STOP scenarios. In CST, concentrations of all the greenhouse gases but CO_2, radiative forcings of all the near-term climate forcers and albedo effects, and fossil CO_2 emissions are kept constant after 2005. In STOP, all these values are set to their preindustrial value after 2005. In both CST and STOP, land-cover change is assumed to be zero after 2005. Land-uses are assumed to be constant after 2005 in CST, and to be zero in STOP.

The above protocol was further adjusted so that, when atmospheric CH_4 concentration deviates from that of the original RCP because of CH_4 emission from permafrost thaw, OSCAR also calculates the associated change in radiative forcing from stratospheric H_2O and tropospheric O_3 (refs [18,36]).

In this study, OSCAR was not run in a probabilistic fashion—we used the default configuration of the model to save computing time. This implies that the full uncertainty of the Earth system is not sampled in this study, just that of the permafrost system under a close-to-median configuration of the rest of the model. The default configuration has an equilibrium climate sensitivity for CO_2 doubling of ~3.2 °C. A comparison of the default and median results for key variables of the model is provided in Supplementary Fig. 8 for our six scenarios and in the case without permafrost thaw. The median results were obtained by running an unconstrained Monte Carlo ensemble of 2,000 elements, as in a previous work[18]. Supplementary Fig. 8 shows that the default and median atmospheric CO_2 and global temperature simulated variables remain close, with a normalized root-mean square error <5%. Two noticeable biases were identified, however. First, the default configuration gives a lower atmospheric CH_4 than the median, which suggests that our results underestimate the additional effect of CH_4 emission caused by permafrost thaw. Second, for RCP2.6 (a peak-and-decline scenario) and to a lesser extent for RCP4.5 (a stabilizing scenario), the default configuration warms more than the median, which indicates that our capture budgets are probably overestimated (which may partly compensate for the protocol-induced underestimate described in the main text).

Permafrost carbon emulator. We coupled a permafrost emulator to OSCAR v2.2.1, calibrated on four land surface models: JSBACH (see below), ORCHIDEE-MICT[19] and JULES[20] following the two different versions DeepResp and SuppressResp[21]. The calibration of the parameters defined hereafter is done using outputs of the complex models for integrations over 1850–2300 of the RCPs 8.5, 4.5 and 2.6. In this emulator, we calibrated and separately ran the permafrost system of two aggregated regions of the globe: North America and Eurasia. In these models, we call 'permafrost carbon' the carbon that was frozen (and therefore inactive) during preindustrial times. All the parameter values are given in Supplementary Table 4.

First, we modelled the regional air surface temperature change (T^i) in each region i with a linear dependency on global temperature change (T):

$$T^i = \omega^i T \tag{1}$$

The parameters ω^i are calibrated with a linear fit between T^i and T (Supplementary Figs. 9 and 10, first row). Note that this parameter represents a feature of the climate system. It does not actually come from the emulated land surface model, but rather from the climate model it uses as the input. In the case of JSBACH, this is the MPI-ESM-LR model's results for CMIP5[57]. In the case of ORCHIDEE and JULES, the detailed protocol of the simulations used is from Burke et al.[21]. For JULES, we took the average of all the realizations made with IMOGEN, and for ORCHIDEE we took only one realization made with IMOGEN emulating HadCM3.

Second, we calibrated the temperature dependency of the heterotrophic respiration rate of non-permafrost carbon (r) following a Gaussian law[58]:

$$r^i = r_0^i \exp(\gamma_1^i T^i - \gamma_2^i T^{i\,2}) \tag{2}$$

γ_1 and γ_2 are the sensitivity parameters calibrated with forced positive values (Supplementary Figs. 9 and 10, second row), and r_0 is the preindustrial heterotrophic respiration rate taken as the average over 1850–1859 in the case of JSBACH, and 1850 in the case of ORCHIDEE and JULES (as IMOGEN features no interannual variability).

Third, we introduced the theoretical thawed fraction ($\overline{p}$) that can take values from $-p_{\min}$ to 1, with a preindustrial value of 0. This corresponds to the fraction of thawed permafrost carbon for a given regional temperature change, but neglects dynamic considerations. It is fitted by an S-shaped function:

$$\overline{p}^i = -p_{\min}^i + \frac{1 + p_{\min}^i}{\left(1 + \left(\left(\frac{1}{p_{\min}^i} + 1\right)^{\kappa_p^i} - 1\right)\exp(-\gamma_p^i \kappa_p^{i} T^i)\right)^{\frac{1}{\kappa_p^i}}} \tag{3}$$

$p_{\min}$ represents a hypothetical (that is, never reached) case of fully frozen soils, κ_p is a shape parameter and γ_p the sensitivity parameter. The three parameters are calibrated with the same fit (Supplementary Figs. 9 and 10, third row), with the additional constraint that $p_{\min}$ cannot be greater than the ratio of the model's non-frozen soil carbon over frozen soil carbon in preindustrial times. In the case of JSBACH, because there is no refreezing in the model, we calibrated this relationship on the scenario with the fastest warming only (that is, RCP8.5). For ORCHIDEE and JULES, the calibration was made with all scenarios. Therefore, the exact physical meaning of $\overline{p}$ depends on the emulated model.

Fourth, we introduced an asymmetric dynamic behaviour in the thawing/freezing process by defining the actual thawed fraction (p), which lags behind the theoretical thawed fraction $\overline{p}$:

$$\frac{dp^i}{dt} = \nu^i(\overline{p}^i - p^i) \tag{4}$$

with:

$$\nu^i = \begin{cases} \nu_{\text{thaw}}^i, \text{if } \overline{p}^i \geq p^i \\ \nu_{\text{froz}}^i, \text{if } \overline{p}^i < p^i \end{cases} \tag{5}$$

ν_{thaw} and ν_{froz} are the speeds of thawing and freezing, respectively. They are calibrated simultaneously with the transient simulations (Supplementary Figs. 9 and 10, fourth row), using equations (3)–(5) driven only by the regional temperature change taken from the emulated model, that is not using equation (1).

Fifth, a frozen carbon pool (C_{froz}) changes with time following the thawing carbon flux (F_{thaw}) calculated as the product of the frozen pool size during preindustrial times ($C_{\text{froz},0}$) by the speed of change in (that is, the time derivative of) the actual thawed fraction:

$$-\frac{dC_{\text{froz}}^i}{dt} = F_{\text{thaw}}^i = \frac{dp^i}{dt} C_{\text{froz},0}^i \tag{6}$$

Inspired by Koven et al.[30], we then split the thawing flux between three thawed carbon pools (C_{thaw1}, C_{thaw2}, C_{thaw3}) following the partitioning coefficients (π_{thaw1}, π_{thaw2}, π_{thaw3}). Note, however, that for some models we reduced the number of thawed carbon pools to avoid overfitting (Supplementary Table 4). Each thawed carbon pool was then subjected to heterotrophic respiration with its own turnover time (τ_{thaw1}, τ_{thaw2}, τ_{thaw3}). The respiration rate is affected by regional temperature change following the same law as in equation (2), except that the sensitivities are modified by a factor κ_{thaw}. This gives:

$$\begin{cases} \frac{dC_{\text{thaw1}}^i}{dt} = \pi_{\text{thaw1}}^i F_{\text{thaw}}^i - \frac{1}{\tau_{\text{thaw1}}^i}\left(\frac{r^i}{r_0^i}\right)^{\kappa_{\text{thaw}}^i} C_{\text{thaw1}}^i \\ \frac{dC_{\text{thaw2}}^i}{dt} = \pi_{\text{thaw2}}^i F_{\text{thaw}}^i - \frac{1}{\tau_{\text{thaw2}}^i}\left(\frac{r^i}{r_0^i}\right)^{\kappa_{\text{thaw}}^i} C_{\text{thaw2}}^i \\ \frac{dC_{\text{thaw3}}^i}{dt} = \pi_{\text{thaw3}}^i F_{\text{thaw}}^i - \frac{1}{\tau_{\text{thaw3}}^i}\left(\frac{r^i}{r_0^i}\right)^{\kappa_{\text{thaw}}^i} C_{\text{thaw3}}^i \end{cases}$$

To ensure mass balance, we must have $\pi_{t3} = 1 - \pi_{t1} - \pi_{t2}$. The other six parameters were calibrated simultaneously with transient simulations by fitting the respiration

flux simulated by our emulator to the actual complex model's flux (Supplementary Figs. 9 and 10, fifth row). To do so, we used only equation (7), driven by the complex model's thawing carbon fluxes and heterotrophic respiration rates.

Finally, the permafrost carbon emissions (E_{pf}) were deduced as:

$$E^i_{pf} = -\frac{dC^i_{thaw1}}{dt} - \frac{dC^i_{thaw2}}{dt} - \frac{dC^i_{thaw3}}{dt} - \frac{dC^i_{froz}}{dt} \quad (8)$$

The overall performance of the emulator is shown in Supplementary Figs. 9 and 10 (sixth row), with the emulator driven only by the emulated model's global temperature change (the only driver of our permafrost module). Overall, the performance of the emulator is very satisfying, with a normalized root-mean square error for global cumulative permafrost carbon emissions of 2.8%, 5.3%, 5.7% and 7.1% for JULES-DeepResp, JULES-SuppressResp, JSBACH and ORCHIDEE-MICT, respectively.

Effect of methane emissions. A fraction of 2.3% (ref. [14]) of permafrost carbon emission is assumed to be CH_4. This value is assumed to remain constant throughout the simulations because the future response of this fraction to environmental changes (for example, climate or CO_2) is unclear[33]. In OSCAR, the atmospheric evolution of these CH_4 molecules is tracked in a separate manner, so that, when the permafrost-induced CH_4 is oxidized in the atmosphere, we add the newly formed CO_2 to the atmospheric CO_2 pool. Therefore, the long-term addition of CO_2 to the atmosphere caused directly by permafrost thaw does not depend on the CH_4 fraction. The transient warming and ensuing feedbacks in the system, however, are a function of this fraction.

To investigate this effect, two additional series of simulations were performed: one without and one with a doubled methane emission (that is, fractions of 0% and 4.6%, respectively). The methane effect shown in Fig. 4 is equal to the difference between the budgets obtained in the main simulations with 2.3% of methane and those obtained in the simulations with 0%. We also found that the difference between the 4.6% and 2.3% simulations is approximately the same as that between 2.3% and 0% (not shown), which suggests the absolute contribution of methane is roughly linear in this domain.

Exceedance budgets protocol. To obtain the exceedance budgets, we ran our six scenarios with the permafrost module turned off and with its four alternative configurations. This is a total of $6\times5=30$ simulations. By definition, for each of these simulations, the exceedance budget is the maximum cumulative amount of anthropogenic CO_2 that is emitted up to the time when the given temperature target is exceeded[22]. So, the exceedance budgets are calculated as:

$$B_{exc} = \max_{\tau} \int_{t_0}^{\tau} E_{FF}(t) + E_{LUC}(t)\,dt \quad (9)$$

for $T(\tau) \le T_{target}$ and where B_{exc} is the exceedance budget, E_{FF} the yearly fossil fuel CO_2 emission, E_{LUC} is the yearly CO_2 emission from land-use change, t_0 the year the simulation starts, T the simulated temperature change and T_{target} the target temperature change.

Fossil fuel CO_2 emission pathways. For the avoidance budgets, we require a set of varied CO_2 emission pathways that cover a wide range of possible futures. We created these emission pathways as the sum of one positive emission pathway and one negative: $E_{FF} = E_{FF+} + E_{FF-}$.

The pathway of positive emission is defined using a parameterized analytical formula of the peak-and-decline form on a semi-infinite interval[59]:

$$E_{FF+} = \begin{cases} E_{FF+}(t), \text{if } t \le t_1 \\ E_{FF+}(t_1)\exp(r(t-t_1)), \text{if } t_1 < t \le t_m \\ F_m(1+(r+m)(t-t_m))\exp(-m(t-t_m)), \text{if } t > t_m \end{cases} \quad (10)$$

where $F_m = E_{FF+}(t_1)\exp(r(t_1-t_m))$. We also defined the total cumulative positive emission (Q_+) of this pathway:

$$Q_+ = \int_{t_0}^{\infty} E_{FF+}(t)\,dt = Q_{t_1} + \int_{t_1}^{\infty} E_{FF+}(t)\,dt \quad (11)$$

Here t_1 is the last year of the historical data, t_m the time at which mitigation begins, r the historical growth rate of fossil CO_2 emissions and m the mitigation rate. The value of r is taken as the mean of the growth rate over the last ten years of the historical period ($r = 0.022623\,yr^{-1}$). The mitigation rate m is deduced from the other parameters:

$$m = \frac{F_m}{A_r}\left(1+\sqrt{1+\frac{A_r}{rF_m}}\right) \quad (12)$$

with $A_r = Q_+ - Q_{t_1+} - \frac{F_m}{r}(1-\exp(r(t_1-t_m)))$. Each positive emission pathway is uniquely defined by the tuple (t_1, t_m, Q_+). In a similar manner, the negative emission pathways are defined following a logit-normal law on a finite interval:

$$E_{FF-} = \frac{Q_-}{x(1-x)}\frac{1}{\sigma\sqrt{2\pi}}\exp\left(-\frac{\left(\log\left(\frac{x}{1-x}\right)-\mu\right)^2}{2\sigma^2}\right) \quad (13)$$

with:

$$x = \frac{t-(t_m+t_{lag})}{t_f-(t_m+t_{lag})} \quad (14)$$

where t_f is the last year of the simulation, μ and σ are two shape parameters, t_{lag} is the time between the start of the mitigation of the positive emissions and that of the negative emissions and Q_- the cumulative amount of negative emissions. Each negative emission pathway is uniquely defined by the tuple (t_{lag}, μ, σ, Q_-).

Using the above equations, we created 520 fossil fuel CO_2 emission pathways by combining different values for the positive emission tuple (t_1, t_m, Q_+) and the negative emission one (t_{lag}, μ, σ, Q_-). A full list of these 520 combinations of parameters is provided in Supplementary Table 5. The obtained emission pathways are also represented in Supplementary Fig. 4.

Avoidance budgets protocol. To calculate the avoidance budgets, we ran simulations with the 520 fossil fuel CO_2 emission pathways combined with the six scenarios we already had for all the other drivers of the model (that is, non-CO_2 forcings and land-use drivers), with the permafrost module turned off and with its four alternative configurations. This led to a total of $520\times6\times5=15{,}600$ simulations. We note that our approach of combining two independent sets of scenarios probably leads to an overestimation of the scenario-related uncertainty, as we implicitly combine inconsistent sources of CO_2 and non-CO_2 emissions[46]. It allows, however, for a systematic analysis of the effect of non-CO_2 forcing (using, for example, Supplementary Table 1).

Then, for each of these simulations (superscript i), we calculated the maximum temperature of the simulation:

$$T^i_{max} = \max_{\tau<t_f} T^i(\tau) \quad (15)$$

and its maximum cumulative CO_2 emissions:

$$B^i_{max} = \max_{\tau<t_f} \int_{t_0}^{\tau} E^i_{FF}(t) + E^i_{LUC}(t)\,dt \quad (16)$$

If any of these two maxima occurred at the last time step of the simulation (t_f), the simulation was discarded. With this approach, we were certain that an emission budget of B_{max} ensures that the global temperature does not go above T_{max}, given the non-CO_2 and land-use forcings of the ith scenario.

However, we have no control over the individual values of T_{max}. Therefore, to deduce the avoidance budgets (B_{avo}) for an exact temperature target, we interpolate linearly in the (B^i_{max}, T^i_{max}) phase space, within the T_{max} value interval of ±0.2 °C around T_{target}. We acknowledge this is not exactly the approach followed Rogelj et al.[46]. However, our approach does respect the philosophy of the 'avoidance' budget in ensuring that the temperature target is, indeed, avoided. Obviously, for a given non-CO_2 and land-use scenario, any budget lower than the deduced B_{avo} also implies avoiding the temperature target.

Net overshoot budgets protocol. Net overshoot budgets (B_{net}) are the combination of two budgets: an emission budget to reach the peak temperature (B_{peak}) and a capture budget that consists of the cumulative amount of negative emission required to go back to the targeted temperature ($B_{cap} < 0$), $B_{net} = B_{peak} + B_{cap}$. Therefore, net overshoot budgets are defined for a given temperature target and a given level of overshoot (T_{over}), with the peak temperature then being given by $T_{peak} = T_{target} + T_{over}$.

To calculate B_{peak} and B_{cap}, we used the same ensemble of scenarios as for the avoidance budgets. In each case, we took only the subset of scenarios whose maximum temperature was ±0.2 °C of the chosen T_{peak} and then declined by at least T_{over}. For each of these scenarios (superscript j), we calculated T^j_{max} and B^j_{max} exactly as we do for the avoidance budgets in equations (15) and (16). We also calculated B^j_{neg}:

$$B^j_{neg} = \min_{\tau} \int_{t_1}^{\tau} (E^j_{FF}(t) + E^j_{LUC}(t))\,[E^j_{FF}(t) + E^j_{LUC}(t) \le 0]\,dt \quad (17)$$

for $T^j(\tau) \ge T^j_{max} - T_{over}$ and using Iverson brackets in the notation (which take a value of 1 if and only if the logical test in the brackets is true, and 0 otherwise.)

Then, just as with the avoidance budgets, we linearly interpolated B_{peak} and B_{cap} in the (B^j_{max}, T^j_{max}) and $(B^j_{neg}, T^j_{max}-T_{over})$ phase spaces, respectively. The net overshoot budget B_{net} is deduced by summation of B_{peak} and B_{cap}. We note again that this protocol, being somewhat similar to the exceedance protocol in its formulation, ignores everything that may occur after the temperature returns below the targeted value. It therefore provides a lower-bound estimate of future capture requirements.

Extra data processing. To be consistent with IPCC[6], we adjusted our budgets for a preindustrial year of 1870. To do so, before actually calculating any budget, global temperatures (T) were offset by a value equal to the average over 1861–1880, and cumulative CO_2 emissions (B) were reduced by the cumulative amount of CO_2 emitted over 1765–1870. Budgets are rounded to the nearest 10 Gt CO_2 in the tables and main text. We also discarded estimates of B_{avo} and B_{peak} for which the coefficient of determination of the linear fit was less than 0.50.

Remaining budgets calculation. The remaining budgets (ΔB) were calculated as $\Delta B = B - B_{hist}$, where B can be B_{exc}, B_{avo} or B_{net}, and B_{hist} is the historical cumulative CO_2 emission from anthropogenic activities (from all sources: fossil fuel burning, industry and land-use changes). We take $B_{hist} = 2{,}240$ Gt CO_2 (ref. [44]). In Fig. 2b, we show the relative reduction in remaining budgets caused by permafrost carbon release, that is, $\Delta B_1/\Delta B_0 - 1$, where the subscript '1' is for a case with permafrost carbon processes, and '0' for one without. In Fig. 3, we show reductions in budgets relative to those in the exceedance case, $\Delta B/\Delta B_{exc}$.

Permafrost in JSBACH. The earlier CMIP5 version of the Max Planck Institute Earth system model land surface scheme JSBACH[60,61] is extended with a multilayer hydrology scheme[62], a representation of permafrost physical processes[63] as well as the improved soil carbon model YASSO[64]. For permafrost carbon stocks, we represented carbon cycling in the active layer by the YASSO model, and we prescribed frozen carbon stocks below the active layer from the Northern Circumpolar Soil Carbon Database (NCSCD) version 2 (ref. [65]). When the active layer thickness changed, we transferred carbon from the prescribed frozen carbon stocks to the active YASSO carbon pools.

Code availability. The source code of OSCAR is available at https://github.com/tgasser/OSCAR. The code used to generate all the results of this study is available from the corresponding author upon request.

Data availability

RCP scenarios are available at http://www.pik-potsdam.de/~mmalte/rcps/. The data that support the findings of this study are available from the corresponding author upon request.

References

50. Sitch, S. et al. Recent trends and drivers of regional sources and sinks of carbon dioxide. *Biogeosciences* **12**, 653–679 (2015).
51. Arora, V. K. et al. Carbon-concentration and carbon-climate feedbacks in CMIP5 earth system models. *J. Clim.* **26**, 5289–5314 (2013).
52. Joos, F. et al. An efficient and accurate representation of complex oceanic and biospheric models of anthropogenic carbon uptake. *Tellus B* **48**, 394–417 (1996).
53. Geoffroy, O. et al. Transient climate response in a two-layer energy-balance model. Part I: analytical solution and parameter calibration using CMIP5 AOGCM experiments. *J. Clim.* **26**, 1841–1857 (2013).
54. Holmes, C. D., Prather, M. J., Søvde, O. A., & Myhre, G. Future methane, hydroxyl, and their uncertainties: key climate and emission parameters for future predictions. *Atmos. Chem. Phys* **13**, 285–302 (2013).
55. Jones, C. et al. Twenty-first-century compatible CO_2 emissions and airborne fraction simulated by CMIP5 earth system models under four representative concentration pathways. *J. Clim.* **26**, 4398–4413 (2013).
56. Hurtt, G. C. et al. Harmonization of land-use scenarios for the period 1500–2100: 600 years of global gridded annual land-use transitions, wood harvest, and resulting secondary lands. *Clim. Change* **109**, 117 (2011).
57. Giorgetta, M. A. et al. Climate and carbon cycle changes from 1850 to 2100 in MPI-ESM simulations for the Coupled Model Intercomparison Project phase 5. *J. Adv. Model. Earth Syst.* **5**, 572–597 (2013).
58. Tuomi, M., Vanhala, P., Karhu, K., Fritze, H. & Liski, J. Heterotrophic soil respiration—comparison of different models describing its temperature dependence. *Ecol. Model.* **211**, 182–190 (2008).
59. Raupach, M. R. et al. The relationship between peak warming and cumulative CO_2 emissions, and its use to quantify vulnerabilities in the carbon–climate–human system. *Tellus B* **63**, 145–164 (2011).
60. Brovkin, V. et al. Evaluation of vegetation cover and land-surface albedo in MPI-ESM CMIP5 simulations. *J. Adv. Model. Earth Syst.* **5**, 48–57 (2013).
61. Schneck, R., Reick, C. H. & Raddatz, T. Land contribution to natural CO_2 variability on time scales of centuries. *J. Adv. Model. Earth Syst,* **5**, 354–365 (2013).
62. Hagemann, S. & Stacke, T. Impact of the soil hydrology scheme on simulated soil moisture memory. *Clim. Dynam.* **44**, 1731–1750 (2015).
63. Ekici, A. et al. Simulating high-latitude permafrost regions by the JSBACH terrestrial ecosystem model. *Geosci. Model Dev* **7**, 631–647 (2014).
64. Goll, D. S. et al. Strong dependence of CO_2 emissions from anthropogenic land cover change on initial land cover and soil carbon parametrization. *Global. Biogeochem. Cycles* **29**, 1511–1523 (2015).
65. Hugelius, G. et al. A new data set for estimating organic carbon storage to 3 m depth in soils of the northern circumpolar permafrost region. *Earth Syst. Sci. Data* **5**, 393–402 (2013).